

Numerical Study of the Influence of Burden Batch Weight on Blast Furnace Performance



XIAOBING YU and YANSONG SHEN

Burden batch weight is a critical operating parameter in the blast furnace (BF) system. It directly affects solid distribution such as coke-layer and ore-layer thickness and thus gas permeability and thermal-chemical conditions inside a BF. However, in the open literature, few quantitative studies have been reported on the influence of burden batch weight on BF performance, such as cohesive zone (CZ) shape and location, reducing gas evolution, and iron oxide reduction behaviors. In this study, a multi-fluid BF model is used to investigate the BF performance with different burden batch weights systematically. This model features the layered burden structure with respective chemical reactions in respective coke and ore layers and a burden batch weight sub-model. The results show that, under the given simulation conditions, with the increased burden batch weight from 112 to 140 tons, the average gas velocity in central regions is significantly suppressed by ~ 1 m/s; the average gas and solid temperatures are decreased by ~ 160 K and the position of CZ decreased by ~ 7 m near the BF center; moreover, the gas utilization efficiency is improved by ~ 2.5 pct; the reduction load of the BF becomes heavier, particularly by ~ 0.05 near the BF center; the fuel rate is decreased by ~ 2.5 kg/thm, meaning a higher furnace efficiency. This study provides theoretical support for batch weight selection and optimization in BF ironmaking practice.

<https://doi.org/10.1007/s11663-020-01924-7>

© The Minerals, Metals & Materials Society and ASM International 2020

I. INTRODUCTION

AN ironmaking blast furnace (BF) is a critical chemical reactor in ironmaking industries. It still dominates iron production because of its high efficiency in terms of energy utilization and iron oxide reduction. In the BF ironmaking process, the solid phase including coke and iron ore is charged alternately at the furnace top. The burden distribution was proved to be capable of improving gas distribution and utilization efficiency in commercial BF practice.^[1] Meanwhile, the hot blast provided by the blower system is injected at the tuyere level to generate the reducing gas. Inside a BF, the counter-current flow of gas–solid–liquid takes place with mass-, momentum- and heat-transfer among them.^[2] From BF dissection results, the burden layer structure was observed to exist until reaching a cohesive zone (CZ).^[3–8] The distributions of solid phase such as burden layer thickness and burden profiles are thus quite vital as they inevitably affect gas flow patterns and the in-furnace thermal-chemical behaviors. Therefore,

solid-phase charging parameters, including batch weight, are recognized as one vitally important approach to tune BF performance not only to ensure the smooth operation but also to obtain a decreased fuel rate and higher efficiency.

Burden batch weight (a quantity of iron-bearing ore charged at one time) is a critical operating parameter in the BF solid-charging system. In practice, it is predominantly determined by the charging capability, including the coke and ore bin volume and bucket volume, and affected by many other factors, such as BF inner volume, raw material quality and in-furnace thermal conditions.^[9] In general, for a BF with a larger volume, a more considerable burden batch weight is chosen compared to a small-scale BF. When the raw materials' quality deteriorates and gas permeability at the furnace center decreases, the burden batch weight can be adjusted to improve the in-furnace conditions. Some qualitative analyses of burden batch weight on BF performance were proposed in the past: when a lower burden batch weight is adopted, the thickness of the coke layer in both the shaft and cohesive zone (CZ) decreases; thus, the resistance for gas flow in coke windows (the coke layers in CZ) increases and more gas flows out through the BF central areas. On the contrary, with an increased burden batch weight, the number of burden layers inside a BF decreases, and the gas flow field can be more uniform because of the increased

XIAOBING YU and YANSONG SHEN are with the School of Chemical Engineering, University of New South Wales, Sydney, NSW 2052, Australia. Contact e-mail: ys.shen@unsw.edu.au

Manuscript submitted March 7, 2020.

Article published online August 10, 2020.

burden layer thickness^[10]; it is reckoned that the change of gas flow pattern brought by batch weight adjustment will lead to different in-furnace phenomena because the gas phase is a carrier of the reducing gas and thermal energy. Specifically, the reduction process of iron ore is driven by many factors, including phase temperature, gas composition, gas pressure, particle size, gas diffusion resistance and chemical reaction resistance. The gas flow patterns with different burden batch weights majorly affect the thermodynamic conditions in terms of temperature field and species distribution and therefore, the reduction process of iron oxides. In general, high temperatures and high concentrations of reductants brought by robust gas flow can lead to fast chemical reaction rates for iron oxide reduction and might help to decrease a BF's fuel rate. However, it is much harder to further deduce specific thermal conditions and chemical behaviors inside a BF.^[11,12] From the above reasoning, it is noted that both a small and a large burden batch weight have their advantages. However, the research to quantitatively characterize those reasonings and hypotheses is lacking in the open literature. Therefore, it is necessary to systematically study the influence of the burden batch weight on BF performance in terms of flow, thermal and chemical behaviors, aiming to deepen the understanding and optimize BF operations.

Many efforts have been devoted to the study of BF burden distribution but mostly to burden profiles at the stockline level only, using experimental and modeling approaches. Some experiments^[13,14] have shown that the burden profiles can be affected by particle physical properties. It is noted that the experimental studies are important, but many are conducted within cold apparatuses with specific conditions and high expense. On the other hand, numerical modeling^[15–18] provides a cost-effective tool to study the BF burden distribution, including the geometric profile, data-driven-based, continuum-based and discrete-based models. Their theory and applications are briefly discussed below. Geometric models are used to study the burden profile at the stockline level.^[12,19–25] For geometric models, the trajectory of charging materials in the discharging process can be solved by analyzing the force balance, including the gravitational force, centrifugal force and sliding frictional force on a single particle. Some phenomena, including the influence of 'scab' on solid flow, are hard to obtain if geometric models are used.^[12,19–25] The data-driven method, such as the neural network, has been used in the prediction of top burden profiles considering the relationship between temperature measurements and burden distributions.^[26,27] However, it is recommended to improve the accuracy of on-line prediction further, especially under innovative operation conditions, for example, pulverized coal injection (PCI) operation and oxygen enrichment operation.^[28] For the continuum-based approach, potential flow theory or viscosity fluid flow theory is used to calculate the burden layer structure inside a BF. This approach features the high efficiency and ability to capture some typical phenomena such as the influence of 'scab' on burden profiles.^[12,29–32] Besides, it should be noted that for the continuum-based approach, the top burden profiles are

required as an input to calculate the in-furnace burden layer structure. The discrete-based method, based on Newton's law of motion, simultaneously handles the translational and rotational movement of all particles and has been proven to be an accurate tool to study the phenomena related to particle flow, such as the BF particle size segregation during the charging process^[11,14,33–35] and the in-furnace burden stress.^[36–38] However, still constrained by computational capacity, this approach does not allow simulating the particle flow in a full-scale BF with a huge particle number.^[37,39–41] However, it is noted that most of the previous research on BF burden distribution focuses on the burden profile/distribution at the furnace top; the effects of burden batch weight, a vital parameter in the charging process, on in-furnace flow-thermal-chemical conditions are seldom studied and discussed.

In this study, a multi-fluid BF model based on our previous work will be used to quantitatively investigate the effect of burden batch weight on typical in-furnace phenomena, including gas flow patterns, CZ formation and thermal-chemical behaviors. The model features different chemical reactions in the respective coke and ore layers and a batch weight sub-model. Moreover, the effects of burden batch weight on BF performance, such as top gas utilization and fuel rate, are predicted and discussed in terms of in-furnace phenomena and key performance indicators.

II. MODEL DETAILS

The present model is based on a recent multi-fluid BF model.^[42] The details of this model and the numerical implementation have been well documented in our previous publications.^[29,42,43] Note that this model features the detailed treatment of layered coke and ore particles and different chemical reactions in the respective layers. It has been validated by comparing the calculation results and experimental measurements of a commercial BF. In this part, the detailed governing equations for flow, heat and mass transfer are not presented for brevity. The model basics and new developments are introduced here for completeness.

A. Model Basics

This model is a two-dimensional (2D) axisymmetric mathematical model in steady state. The calculation domain is above the slag surface in the hearth to the stockline near the furnace top. The layered structure of the solid phase is considered with respective chemical reactions in different burden layers. In this study, Navier–Stokes (N–S) equations are adopted to describe the reducing gas mixture flow field. A Semi-Implicit Method for Pressure Linked Equations (SIMPLE) scheme is adopted to decouple the velocity–pressure field. In addition, the solid phase is treated as one viscous fluid,^[44] and a force balance model^[45,46] is adopted in liquid flow simulation. Heat exchange and momentum transfer among gas, solid and liquid phase are also considered in previous

publications.^[29–31,42,43,46–49] The chemical reaction rate of iron-bearing ore reduction by CO and H₂ refers to Muchi's work.^[50] Specifically, the reaction model assumes that three steps, including diffusion through gas film, intra-particle diffusion and a chemical reaction on the reaction interface, occur steadily and successively during the reaction. In the expression, the chemical equilibrium constant is used to derive the 'driving force' (specie concentration under equilibrium state minus specie concentration under local state) for chemical reactions. Note that the value of the chemical equilibrium constant varies with temperature. These reaction rates provide the basis for mass source or sink calculation for the N–S equation and scalar (*i.e.*, the mass fractions of CO, H₂, CO₂ and H₂O) equations. In addition, some other key reactions, including carbon solution reactions, water gas reactions and water gas shift reactions, are also considered in this model.^[2] For gas inlet boundary conditions, raceway combustion is implicitly considered as in many References 51–55; that is, the flame temperature and components of reducing gas are calculated based on the pre-calculated mass and heat balance. For the treatment of CZ, its profile is determined by the solid phase temperature range, where the typical values for most iron ores, *viz.* 1473 K to 1673 K, are adopted in this work. In particular, the shrinkage ratio, related to solid temperature, is used to represent the softening and melting status of iron-bearing materials. As such, the cohesive process and shrinking index are calculated according to the shrinkage ratio.^[54] The ideal gas equation is used to calculate the density of the reducing gas mixture. Then, the updated gas density is used in the calculation scheme of N–S equations.

B. New Developments of the Batch Weight Sub-model

This research focuses on the study of the influence of burden batch weight on BF performance from a theoretical viewpoint. Thus, for simplicity, the complex behaviors of particle flow and detailed charging patterns are not considered in this work. To quantify the effects of batch weight on BF performance, however, it is necessary to characterize the burden profile at the stockline before the simulation. In this work, the distribution of coke layers and ore layers is described, as shown in Figure 1. Also, the linear burden profiles can be found in related BF modeling works^[54,56] where the volume ratio of ore/(ore + coke) is assumed to change linearly from the furnace center to the wall, as the measurements of such industrial data are quite hard to obtain if not available. The solid layer distribution can be calculated using the timeline of solid flow, as described in References 42, 54. Here, the advantage of the previous burden layer structure model is used to solve the particle distributions inside the BF, adopting different burden batch weights. The equations listed below are derived and then used to calculate the primary parameters of the top coke and ore layers.

$$V_{\text{coke}}^* = R^2 H_1 + 0.5 R^3 t g \alpha \quad [1]$$

$$V_{\text{ore}}^* = R^2 H_2 + 0.5 R^3 t g \alpha \quad [2]$$

$$V_{\text{coke}}^* = M_{\text{coke}} / (\pi \rho_{\text{coke}}) \quad [3]$$

$$V_{\text{ore}}^* = M_{\text{ore}} / (\pi \rho_{\text{ore}}) \quad [4]$$

$$M_{\text{coke}} = M_{\text{ore}} \times \omega_{\text{Fe,ore}} \times \eta \quad [5]$$

$$\rho_{\text{coke}} = \rho_{\text{coke}}^* \times (1 - \varepsilon_{\text{coke}}) \quad [6]$$

$$\rho_{\text{ore}} = \rho_{\text{ore}}^* \times (1 - \varepsilon_{\text{ore}}) \quad [7]$$

$$\varepsilon_{\text{coke}} = 0.153 \times \log_{10} d_{\text{coke}} + 0.724 \quad [8]$$

$$\varepsilon_{\text{ore}} = 0.403 \times (100 \times d_{\text{ore}})^{0.14} \quad [9]$$

where α is the inclined angle of the coke pile, R , V_{coke}^* , V_{ore}^* , M_{coke} , M_{ore} , $\omega_{\text{Fe,ore}}$, η , ρ_{coke} , ρ_{ore} , ρ_{coke}^* , ρ_{ore}^* , $\varepsilon_{\text{coke}}$, ε_{ore} , d_{coke} and d_{ore} are the furnace throat radius, scale-down coke batch volume, scale-down ore batch volume, coke batch weight, ore batch weight, mass fraction of iron element in iron ore, coke ratio, bulk density of coke, bulk density of ore, coke particle density, ore particle density, void fraction of coke pile, void fraction of ore pile, coke particle diameter and ore particle diameter, respectively. Once the values of the basic parameters mentioned above are determined, the volume fractions of coke- and ore-burden layers can be derived. Then, they can be used as the boundary conditions of solid flow and subsequent simulations. This provides an approach to quantitatively investigating the influence of different batch weights on BF performance. Note that, by tuning the parameters of the rotary top chute system, many burden profiles and distributions can be achieved because of the flexibility of the charging system. To ensure a smooth operation, the volume fraction ratio of coke to ore is relatively large near BF central regions. This study focuses on the effect of burden batch weight on the BF inner phenomena below the stockline at the furnace top. The detailed process of material addition and the distribution system above the stockline is beyond the scope of this article.

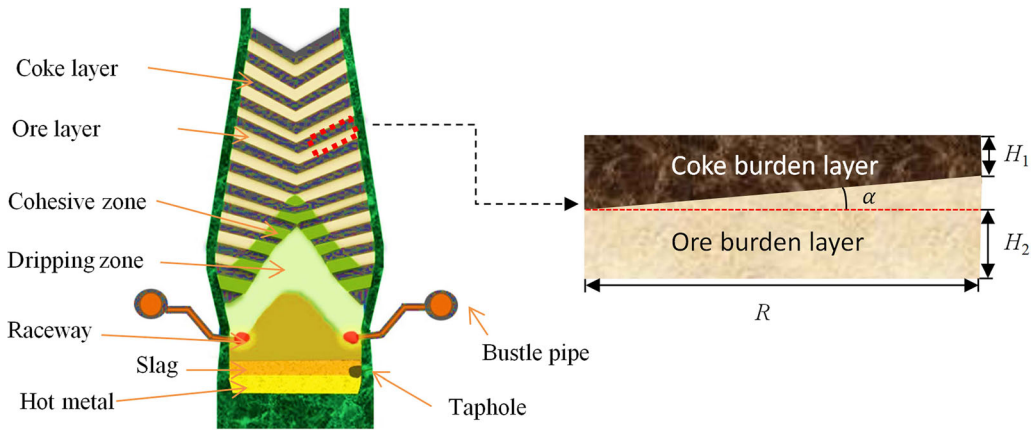


Fig. 1—Schematic of burden distribution in this model.

III. SIMULATION CONDITIONS

The detailed simulation conditions are listed in Table I. In this research, three cases with different batch weights are studied. The chosen batch weight of ore burden is 112 tons (Case 1), 126 tons (Case 2) and 140 tons (Case 3), respectively. For comparing the results quantitatively, bosh gas volume and flame temperature are fixed in this study. Note that the PCI rate is 0.17 ton/thm, *i.e.*, 170 kg/thm. For the coke rates, an initial value (310 kg/thm) is used at the start of the calculation, and then a new value will be predicted and reused in the iteration until the convergence of the calculation. The body-fitted method is used in mesh generation. For capturing the layered structure of the solid phase and minimizing calculation error caused by a coarse grid, dense mesh with a relatively regular nodal distance is generated. The node numbers along the furnace radial direction and furnace axial direction are 131 and 532, respectively. The total mesh number is 68,370, and the average mesh size is around $5.0 \times 5.5 \text{ cm}^2$. This mesh set has a relatively high resolution to capture the in-furnace phenomena.^[42] Besides, mesh independence is studied, indicating that a finer mesh has little impact on the simulation results relative to the mesh used. For quantitatively comparing the difference of BF performance adopting different burden batch weights, three vertical lines for data probing are set at the radius of $x = 0, 2$ and 5 , respectively. The computational domain, monitoring lines and mesh near the furnace top are shown in Figure 2. Considering the particle piled feature as well as for simplicity, in this study, the inclined angle of the interface between the coke and ore layer is set as a constant. As a result, the particle mixing^[11] and push effects^[35] will not be considered in this work.

IV. RESULTS AND DISCUSSION

In this section, the influence of ore batch weight on the BF performance is quantitatively studied in terms of in-furnace phenomena, including flow fields, temperature fields, gas species distributions, reduction degree distributions and key performance indicators including the top gas utilization efficiency and fuel rate.

A. In-Furnace Phenomena

1. Flow patterns

Figure 3 shows the gas flow field of the three cases with different batch weights. For better visualization and comparison, the same range of gas velocity is chosen from 0 to 30 m/s. In general, a relatively high gas velocity is observed near the tuyere level because of the high-speed blast injected through the tuyere. Then, the gas flows towards both the central furnace regions and the top outlet, as can be seen from the gas streamlines. It is noted that the gas flow pattern is affected not only by the burden structure in the shaft but also by the location of CZ. The different void fractions in the respective coke- and ore-burden layers should be the main reason. For example, the coke layers inside the CZ (termed coke windows) have relatively high porosities and can redirect the gas flow towards periphery regions. On the other hand, Figure 3 shows that the gas flow pattern is quite different across the furnace regions. In Case 3, the gas velocity in central regions under the CZ is clearly smaller than in the other two cases, indicating a large batch weight can lead to a relatively less robust central gas flow. The dark blue area in Figure 3 represents the region with a relatively low gas velocity. Therefore, the reduced dark blue area means the increased gas velocity. Comparing Figures 3(c) with (a), it is found that for the

Table I. Simulation Conditions of this BF Model

Parameters	Values
Gas	
Bosh Gas Volume Flux (Nm ³ /thm)	1436
Blast Temperature (K)	1473
Oxygen Enrichment (pct)	1.7
Moisture (g/Nm ³)	8.036
Top Gas Pressure (Atm)	2
Reducing Gas Components (pct)	CO 35.60; N ₂ 59.47; H ₂ 2.0; H ₂ O 0.0; CO ₂ 0.0
Solid	
Burden Batch Weight (Tons)	case 1: 112; case 2: 126; case 3: 140
Ore Rate (Ton/thm)	1.597
Average Ore Components (Pct)	total Fe 59.93
Coke Main Components (Pct)	C 86.794; ash 12.162; S 0.594
PCI Rate (Ton/thm)	0.17
Initial Coke Rate (Ton/thm)	0.31
Coal Main Components (pct)	C 75.3; ash 14.78; S 0.36
Flux Rate (Ton/thm)	0.089
Flux Main Components (pct)	gangue SiO ₂ 92.37 limestone CaO 54.93; CO ₂ 43.06 dolomite CaO 32.38; MgO 19.95; CO ₂ 45.42
Solid Inlet Temperature (K)	300
Void Fraction of Coke Piles (-)	$0.153 \log d_{\text{coke}} + 0.724$
Void Fraction of Ore Piles (-)	$0.403(100d_{\text{ore}})^{0.14}$
Coke Average Diameter (m)	0.045
Ore Average Diameter (m)	0.03
Inclined Angle (Deg)	5
Hot Metal	
Main Components (pct)	Fe 95.369; C 3.805
Density (kg/m ³)	6600
Viscosity (kg/m s)	0.005
Conductivity (W/m K)	28.44
Surface Tension (N/m)	1.1
Slag	
Basicity (-)	B_2 1.23; B_3 1.412; B_4 0.982
Density (kg/m ³)	2600
Viscosity (kg/m s)	1
Conductivity (W/m K)	0.57
Surface Tension (N/m)	0.47

thm stands for a metric ton (equals to 1000 kg) of hot metal.

lower BF regions, particularly those near the furnace bosh wall, the dark blue area reduces, indicating the gas velocity near the furnace wall increases and different effects of burden batch weight on the gas flow pattern in different regions.

Quantitatively, Figures 4(a) through (c) compares the gas velocity development along three vertical lines, *viz.* $x = 0$, $x = 2$ and $x = 5$, respectively. Overall, the curves show fluctuation trends, especially in the shaft, because of the burden layer structure; the extreme peaks and valleys on those curves occur when the gas flows inside the CZs. Comparing Figures 4(a) and (b), near the furnace center, shows that in the height range of 0 to 5 m, the velocity of case 3 is lower than those of Case 1 and Case 2 (the velocity difference can be ~ 5 m/s at some points), indicating the development of central gas can be weakened with a large burden batch weight. On the other hand, Figures 4(c), near the furnace wall, shows the velocity of Case 3 is higher than those of the others when the height is around 0, *viz.* near the tuyere level. This phenomenon indicates the gas flow near the low-periphery regions gets enhanced as a large burden batch weight is adopted. In addition, with the increased burden batch weight, the gas flow field in the shaft can become much smoother with smaller fluctuations, as shown in Figures 4(a) through (c). To be specific, the standard deviations of gas velocity probed at heights > 10 m and along the furnace axis are calculated and are 1.820 for Case 1, 1.421 for Case 2 and 1.265 for Case 3, respectively.

To make an overall comparison among the three cases, the gas velocity along the furnace radial direction is averaged and plotted in Figure 4(d). To calculate the average gas velocity along the furnace radial direction, the BF domain is evenly divided into 40 sections, while each section is located in a range of its radii. Then, the data including gas velocity and x -coordinates in each section will be averaged. For example, the average gas velocity in each section is calculated based on:

$$\overline{\text{vel}} = \sum_i^N \text{vel}_i / N \quad [10]$$

where vel_i is the gas velocity magnitude in the i -th cell of the section, and N is the number of the cell of the section. Figure 4(d) shows that the average gas velocity distribution curves under three cases have a similar trend, namely, they all decrease gradually along the furnace radial direction. To be specific, the average gas velocity on furnace axis is relatively large, *viz.* the central gas has been developed. This is because larger volume ratios of coke to ore are set near the BF central regions than near the furnace wall, as shown in the schematic of the burden profile (Figure 1). Another point is that, for each curve, a respective peak and a respective valley of gas velocity exist. Those peaks are formed by the relatively high gas velocity around the raceway. Besides, it is noted that with the increased batch weight, the average gas velocity gradually decreases, especially in the radii range from 0 to ~ 6.5 m. The closer to the furnace center, the larger the velocity difference is. To be specific, at the furnace center, the average gas velocity difference is near 1.0 m/s, comparing Case 1 with Case 3, indicating that the central gas flow can be effectively suppressed by the increased batch weight. Besides, it is also noted that

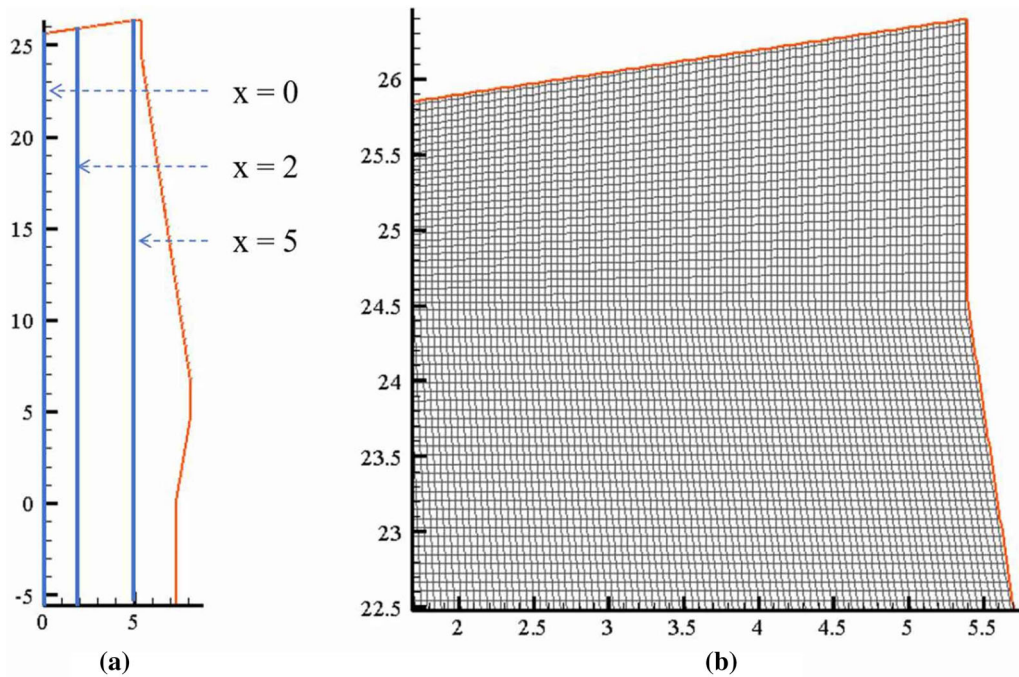


Fig. 2—(a) BF geometry profile and (b) a sectional mesh near the furnace top.

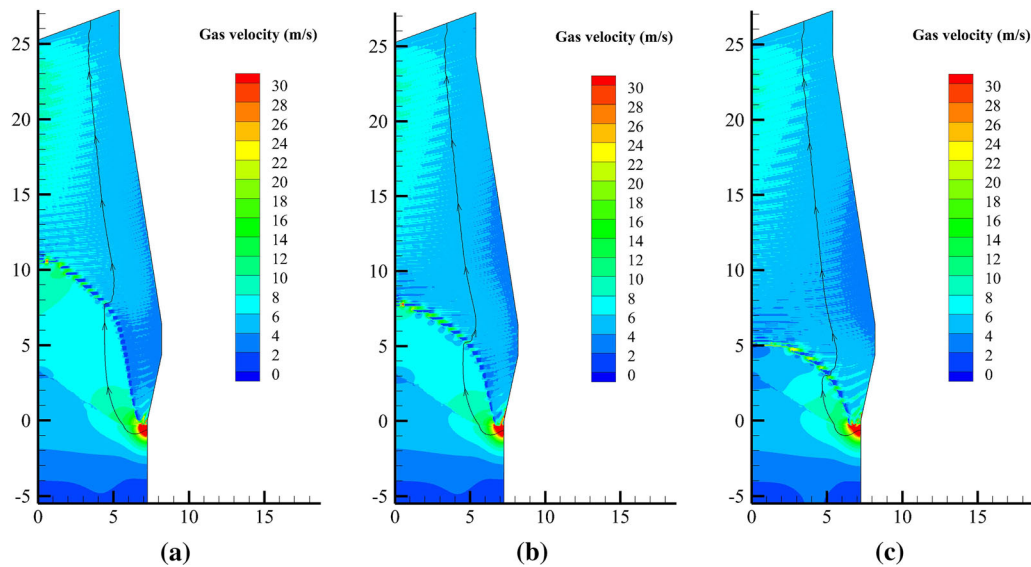


Fig. 3—Gas flow patterns of the three cases with different burden batch weights: (a) Case 1: 112 tons; (b) Case 2: 126 tons and (c) Case 3:140 tons.

the curves have the trends, *viz.* the closer to the furnace center or furnace wall, the more significant the velocity difference. For example, compared with Case 1 and Case 3, a gas velocity difference of ~ 1.0 m/s can be observed at the furnace wall. To be more quantitative, compared to Case 1, the gas flow rate along the furnace axis of Case 3 can be decreased by 14.8 pct; on the other hand, the gas flow rate near periphery regions of Case 3 is roughly increased by 33.3 pct. This indicates that a well-developed periphery flow gas

in the bosh region can be anticipated when the BF adopts a large batch weight. The reasons behind this phenomenon include, first, that with the increased batch weight, gas flow resistance in coke windows decreases; therefore, more gas is expected to flow towards furnace wall through coke windows rather than towards central furnace regions; second, the gas mass flow rate is fixed in this study; thus, with a decreased central gas flow rate, the periphery gas flow rate increases. The gas flow field provides a basic

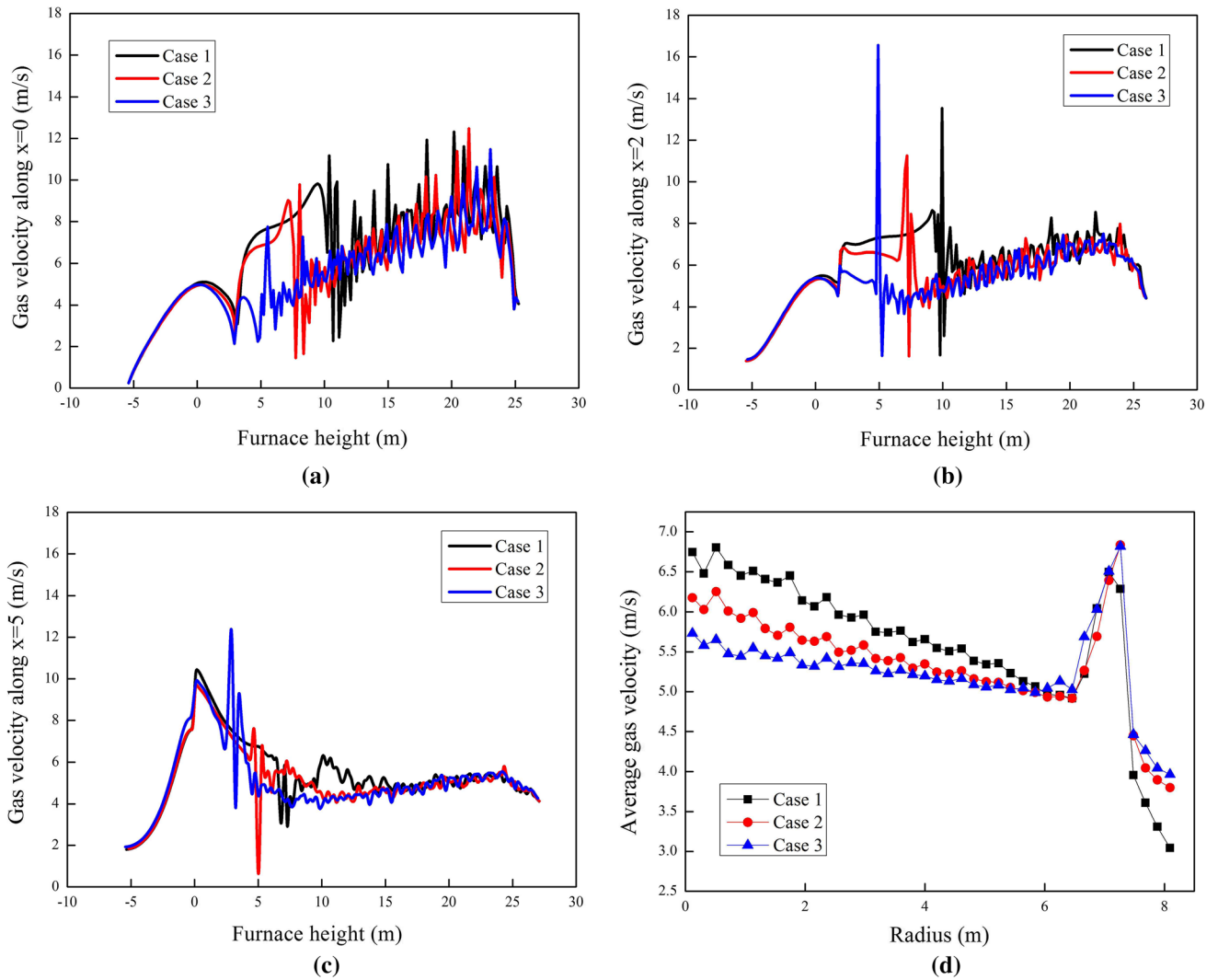


Fig. 4—Gas velocity evolution: (a) to (c) along the lines of $x = 0$, $x = 2$ and $x = 5$ and (d) the average gas velocity along the furnace radial direction.

understanding of the inner phenomena and can help estimate the furnace stability under different burden batch weight conditions.

2. Thermal behavior

Figures 5 and 6 show the gas temperature and solid temperature of the three cases, respectively. The thermal conditions of the different cases show a similar distribution on the whole, *viz.* gas temperature is always higher than solid temperature. This is mainly because of the counter-current flow conditions of gas and solid phases and the endothermic chemical reactions in the local areas. Under the different batch weights, the distributions of isothermals of both solid and gas phase are quite different around the CZs; however, the difference is not significant in the upper shaft. With the increase of batch weight, the high-temperature regions of both gas phase and solid phase decrease, and the regions above CZ, *viz.* low-temperature regions,

expand. Therefore, it is expected that the region for indirect reduction increases while that for direct reduction decreases, which will be further elaborated quantitatively in the next section related to the CZ profile. Additionally, the features of fluctuating isothermals can be observed because of the different physicochemical properties, such as density and thermal capacity, in the respective coke- and ore-burden layers.

Figure 7 shows the distributions of average gas temperature and the average solid temperature along the radial direction under the different batch weight selections. The calculation procedure is similar to Eq. [10], where the velocity term is replaced with the corresponding phase temperature. Figure 7 shows that all the curves have a similar distribution, that is, relatively high temperatures exist near BF central regions. This is because of the development of central gas flow, bringing abundant thermal energy to the furnace center. On the other hand, both the average

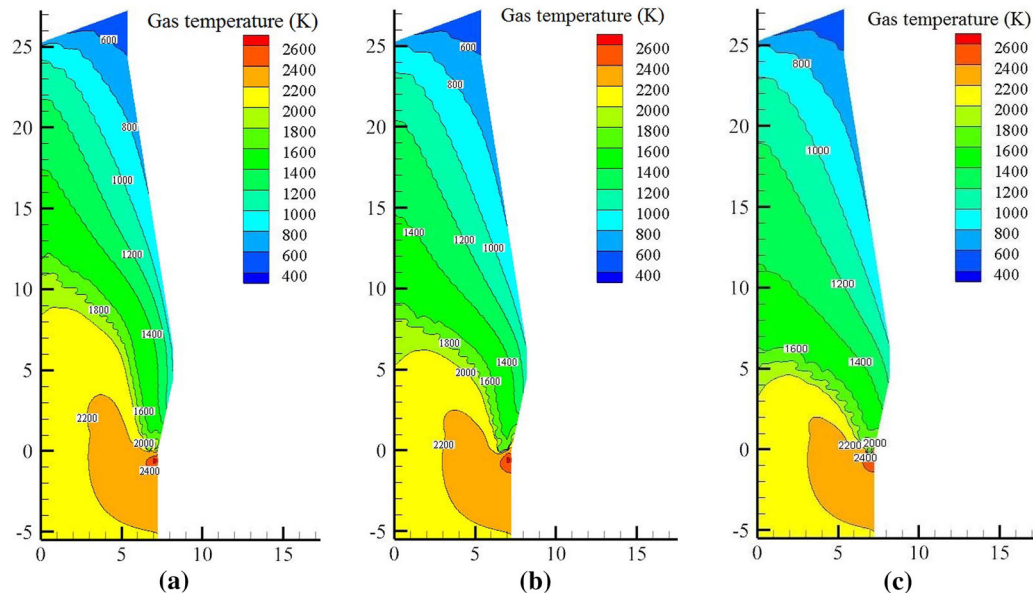


Fig. 5—Gas temperature fields of the three cases with different burden batch weights: (a) Case 1: 112 tons; (b) Case 2: 126 tons and (c) Case 3: 140 tons.

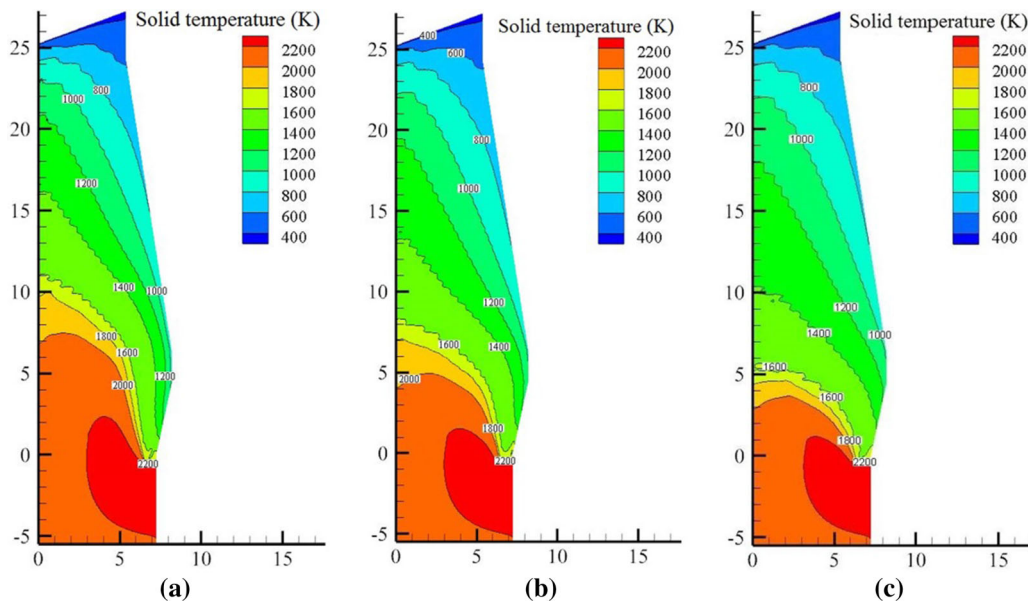


Fig. 6—Solid temperature fields of the three cases with different burden batch weights: (a) Case 1: 112 tons; (b) Case 2: 126 tons and (c) Case 3: 140 tons.

gas and solid temperatures decrease with increased batch weight, which is consistent with the expansion of low-temperature regions as discussed for Figures 5 and 6. Also, it is noted that the influence of batch weight on furnace temperature is more significant near the furnace center rather than near the furnace wall. Specifically, a decrease of about 160 K for both the gas and solid phases is observed at the furnace center. However, near the furnace wall, there is no clear temperature difference among the three cases. The

maximum average temperatures are attained at a radius of 7.2 m because of the high temperature in the raceway. Another point worth mentioning is that the temperature valleys appear at the radius of ~ 5 m, different from the gas velocity valleys (Figure 4). It is indicated that although the temperature fields are closely related to the gas flow patterns, the relationship between them might not be a linear because of the complex flow-thermal-chemical behaviors inside a BF.

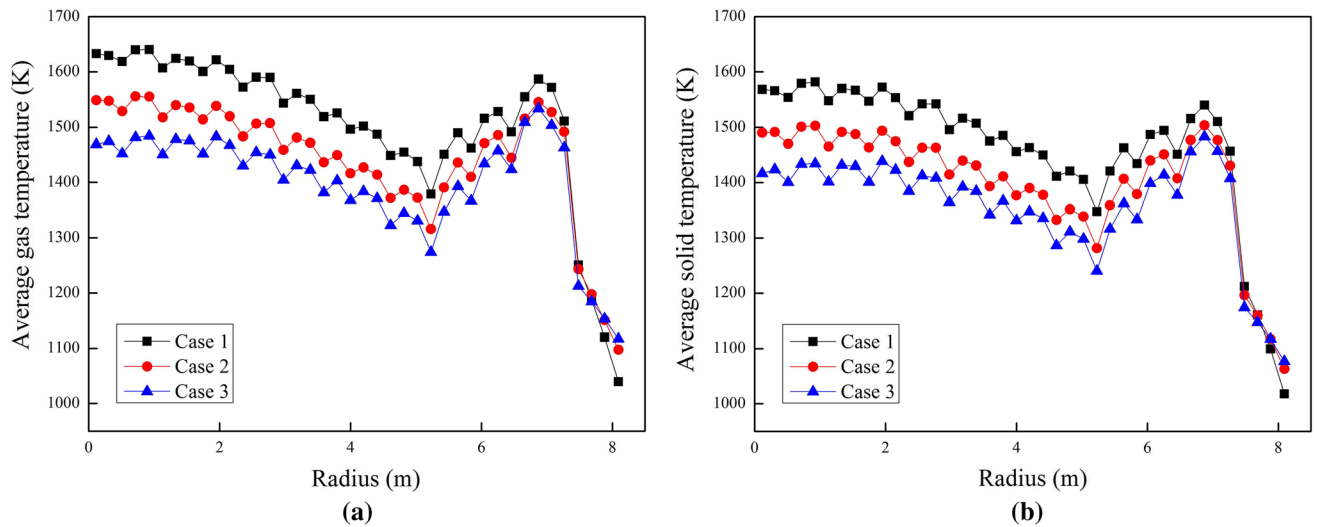


Fig. 7—Trends of average gas temperature (a) and average solid temperature (b) along the furnace radial direction.

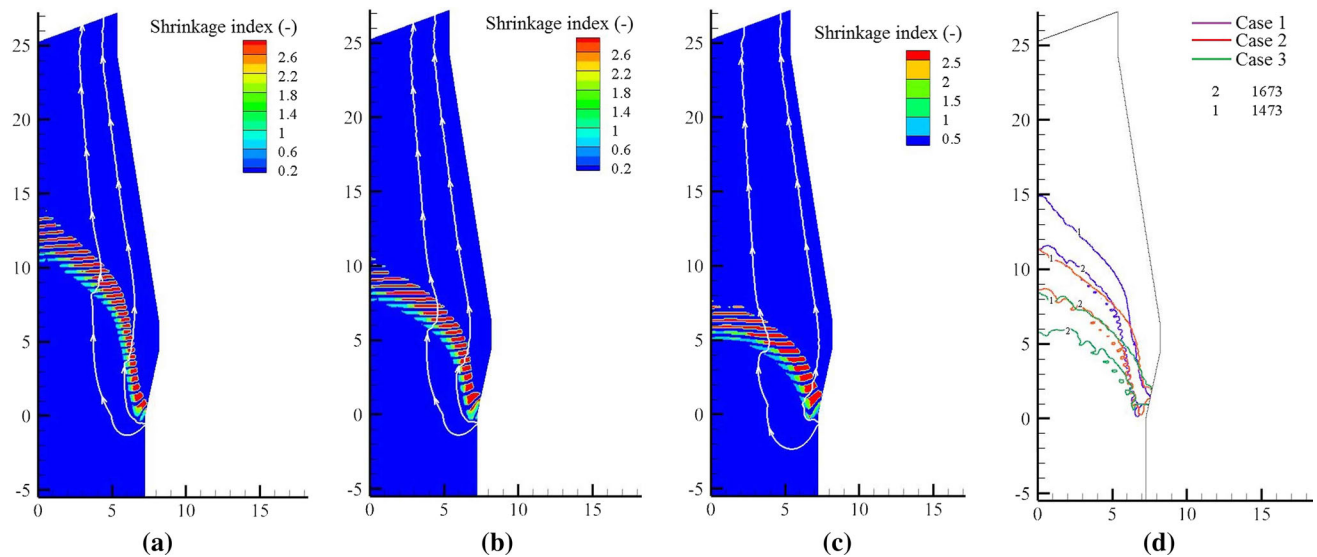


Fig. 8—CZ profiles of the three cases with different burden batch weights: (a) Case 1: 112 tons; (b) Case 2: 126 tons, (c) Case 3:140 tons and (d) CZ comparison.

3. Cohesive zone (CZ) profile

Figure 8 shows CZ's shape and location of the three cases. The CZ is an important region where ore starts to melt, and liquid iron is produced. Thus, it functions as a gas redistributor to change the flow directions of the reducing gas. In this study, different shrinkages of iron oxides (see Figures 8(a) to (c)) related to the iron-bearing ore cohesive process are considered. The different porosity and thermal properties under different stages are set according to References 30, 54. Figures 8(a) to (d) shows that the ore batch weight produces significant effects on the CZ's distribution. With a small batch weight, it is expected that the CZ will move upward towards the stockline level. On the contrary, with a large burden batch weight, the position of the CZ clearly descends, particularly near the furnace center, as shown

in Figure 8(d), indicating the decreased thermal load near the furnace center. It is observed that the height difference of the CZs can be as high as ~ 7 m between Case 1 and Case 3.

To quantitatively demonstrate the influence of ore batch weight, the local volume fractions of the regions above, below and inside the CZs are calculated respectively and plotted in Figure 9. It can be clearly seen that with the increase of ore batch weight, the volume percentage of the above-CZ region gradually increases from 54.46 to 65.26 pct, an increase of 10.8 pct, while the volume percentage below the CZ region decreases from 35.28 to 26.19 pct, a decrease of 9.09 pct. Nevertheless, the CZ volume shows no obvious change, with a slight decrease of 1.71 pct observed. It is indicated that the position of the cohesive zone is quite sensitive to the

change of ore batch weight. When a large burden batch weight is adopted, it is anticipated that the central gas flow will be suppressed because of the lower position of the CZ. The trends, as shown in Figure 9, indicate that if a very heavy burden batch weight is adopted, the CZ might fall upon on the surface of the stagnant region. Consequently, the central gas flow can be affected or cut off. Under such circumstances, the smooth smelting process near the furnace center cannot be achieved, and the un-reacted iron oxides might accumulate in the central furnace regions. On the other hand, if a light batch weight is adopted, it is expected that the CZ can move upwards, resulting in a well-developed central gas flow (see Figures 4 and 8(a)) and a higher top gas temperature (see Figures 5 to 7). Furthermore, the chemical reaction of iron oxides occurring above the CZ is mainly related to the indirect reduction while that in and below the CZ is related to the direct reduction. Comparing Case 3 with Case 1, it is anticipated that the volume percentage of the indirect reduction region can have a 10.8 pct increase while that of the direct reduction region can have a 9.09 pct decrease.

4. Reducing gas

Figure 10 shows the in-furnace CO distribution of the three cases. It is observed that, overall, the concentration of CO decreases when the gas mixture flows towards the furnace center and furnace top. This is because the reduction process where the oxygen element in iron oxides is gradually combined with CO to produce CO₂. The fluctuating trends of the CO concentration are observed resulting from the burden layer distribution considered in this BF model where different burden layers can function as different source or sink for the reducing gas species. Besides, the fluctuating trends show some new features with the increase of ore batch weights. Specifically, for a heavy burden batch weight operation, the fluctuating trends become more obvious. This is because the ore layer of a heavy burden weight is thicker; thus, the effects of layer functioning as a source or a sink on gas components become more significant compared with smaller burden weights.

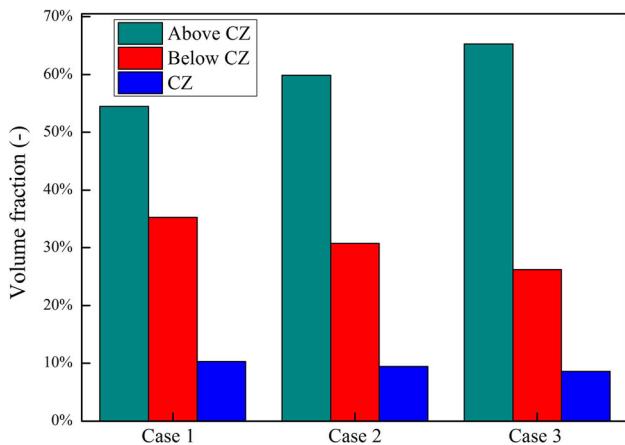


Fig. 9—Region volume fractions of the three cases with different burden batch weights: (Case 1), 112 tons; (Case 2), 126 tons and (Case 3), 140 tons.

Figure 11 shows the CO₂ distribution of the three cases, respectively. Because CO₂ and CO are products and reactants of iron oxide reduction, their distributions show the opposite trends. The concentration of CO₂ gradually increases and reaches the highest level near the furnace throat. Also, the fluctuating patterns of iso-lines can be observed in Figure 11. The distribution of dense iso-lines is observed in the furnace shaft and near the CZ because of the fast reduction process, such as an indirect direction by CO and direct reduction by carbon, which exists in those regions. Therefore, the distribution of CO₂ should be mainly affected by the reduction of iron oxide. On the other hand, the reduction of SiO₂ and decomposition of limestone and dolomite also play roles in the distribution of CO₂ but should be relatively limited because of the limited amount of flux and silicon oxides compared to that of iron oxides. Below the CZ, it is noted that the concentration level of CO₂ is quite limited because the thermal-chemical conditions are disadvantageous for CO₂ existence. Besides, with the increased burden batch weight, the areas of regions with low CO₂ concentration decreases, implying the better utilization of CO. The reason should be the declination of the average in-furnace temperature, which will promote the indirect reduction of iron oxides by CO, an exothermic chemical reaction.

For better comparison, the molar fractions of the top CO and CO₂ of the three cases are plotted, as shown in Figure 12. Particularly in Figure 12(a), Case 1 shows the highest CO concentration (~27 pct) near the furnace center and the lowest CO (~20.5 pct) near the furnace wall. Interestingly, Case 3 shows some different features compared with Case 1. This indicates the CO near the BF central regions can be better utilized with a heavier burden batch weight. As a supplement, in Figure 12(b), the CO₂ in Case 3 shows the highest level (~19.2 pct) near the furnace center, followed by Case 2 (~15.7 pct) and Case 1 (~14.3 pct). In periphery regions, it is noted that Case 3 still ranks the highest (~23 pct) while the curves of Case 1 and Case 2 crisscross with each other at a radius of about 2.5 m. It is observed that the curves can intersect with each other at different furnace radii because the distributions of CO₂ and CO in top gas can be affected by the development of iron oxide reduction inside a BF. It is indicated that, under different burden batch weights, the BF reducing gas might have various features of the trends, such as the slopes along the radial direction.

Figure 13 shows the gas utilization efficiency, one vital smelting index of BF ironmaking, across the calculation domain of the three cases. It is noted that these cases have a similar distribution of this smelting index. It is observed that the utilization of reducing gas gradually increases with the gas flowing towards the furnace top. Moreover, with the increased ore-burden batch weight, the region of gas efficiency > 45 pct becomes more extensive, as clearly shown in Figure 13(c). It is indicated that the overall utilization of the reducing gas can be improved when a BF adopts a heavy ore batch weight.

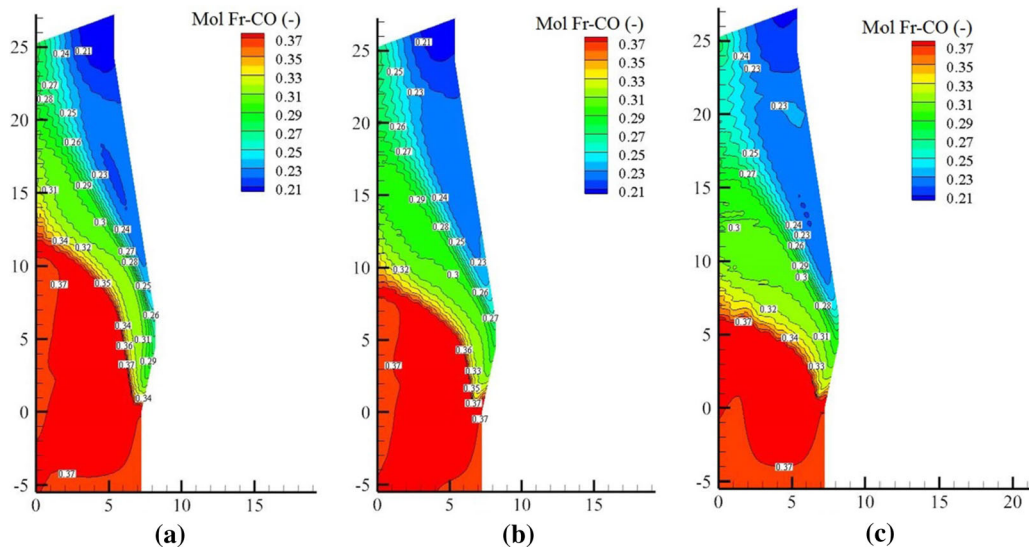


Fig. 10—CO distributions of the three cases with different burden batch weights: (a) Case 1: 112 tons; (b) Case 2: 126 tons and (c) Case 3:140 tons.

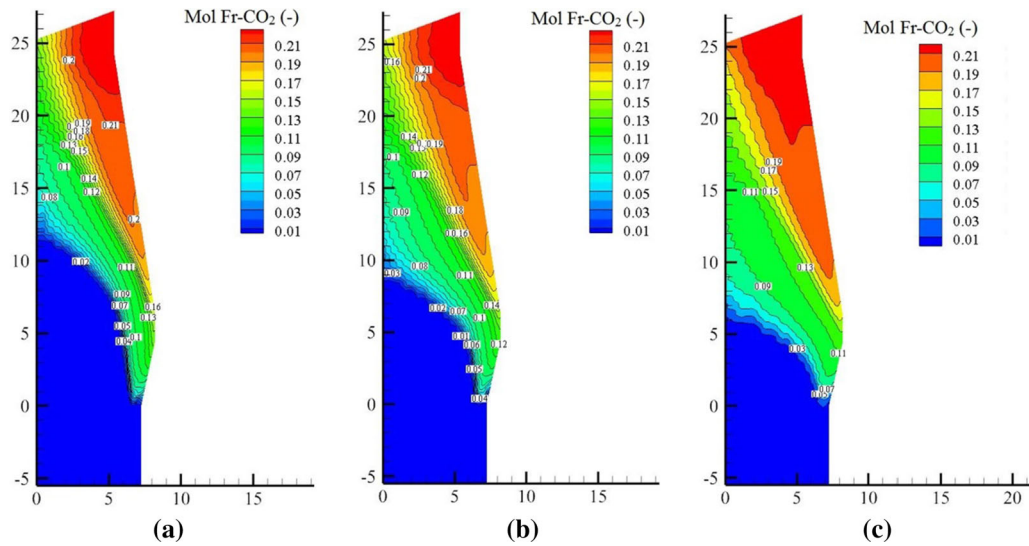


Fig. 11—CO₂ distributions of the three cases with different burden batch weights: (a) Case 1: 112 tons; (b) Case 2: 126 tons and (c) Case 3:140 tons.

Figure 14 shows the top gas utilization along the radial direction and the respective average values of the three cases. As shown in Figure 14(a), the top gas utilization gradually increases along the radial direction and reaches the respective plateau at roughly half of the furnace radius. Then, the curves show insignificant variations towards the furnace wall. The average top gas utilization efficiencies of the three different batch weights are 47.2, 47.8 and 49.7 pct, respectively (Figure 14(b)). An increase of ~ 2.5 pct for the gas utilization efficiency is observed when the burden batch weight increases from 112 to 140 tons. It clearly shows the advantage of adopting a heavy batch weight.

Additionally, the reducing gas is generated from fuel combustion; thus, the well-utilized reducing gas implies a declining level of the fuel rate.

5. Iron oxides reduction

To investigate the reduction behaviors of iron oxides inside a BF, the reduction degree distributions of the three cases are plotted in Figure 15. The isothermals of the solid phase are given to show the relationship between the temperature and reduction degree. Overall, the reduction degree of different cases shows a similar distribution, that is, gradually increases when flowing downward and keeps relatively stable in each chemical reserve zone.^[30,42] The chemical behaviors of iron oxides are mainly determined by the in-furnace temperature,

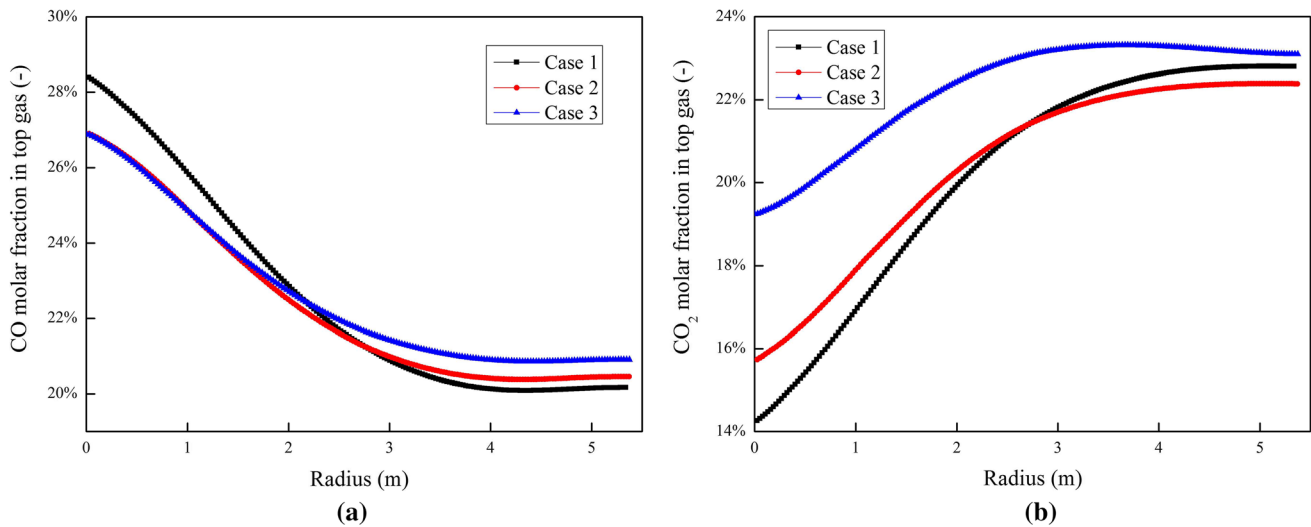


Fig. 12—Evolution of CO (a) and CO₂ (b) on the BF top surface along the furnace radial direction.

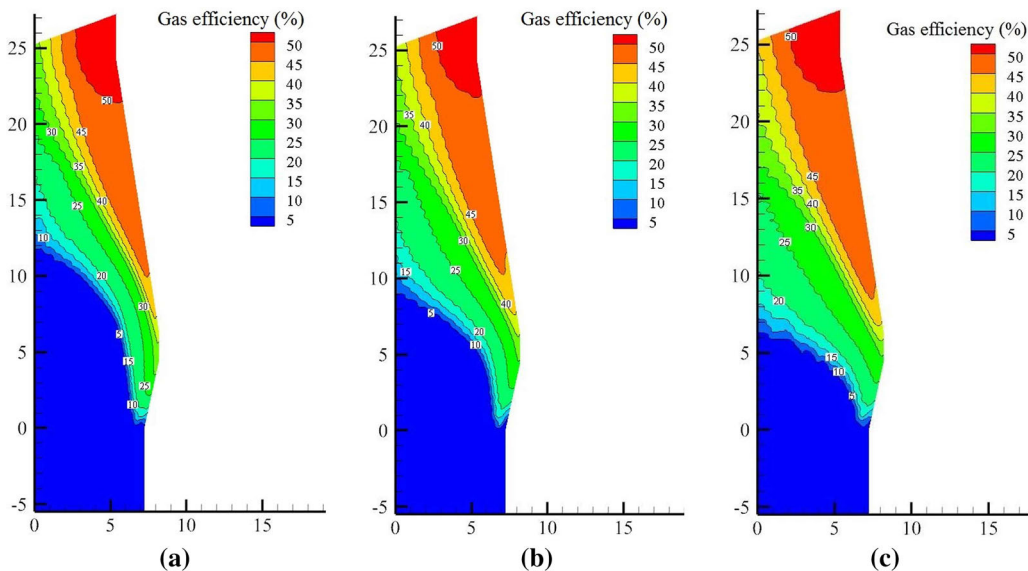


Fig. 13—Gas utilization efficiencies of the three cases with different burden batch weights: (a) Case 1: 112 tons; (b) Case 2: 126 tons and (c) Case 3: 140 tons.

pressure and gaseous reductant concentrations.^[57] Therefore, the change of thermodynamic and kinetic conditions with different burden batch weights will change the distribution of the reduction degree of iron oxides. On the other hand, the solid layer number decreases because of the increased ore batch weight, which would increase the burden layer thickness. Besides, the isothermals inside the BF decline with the increased burden batch weight and affect the reduction behaviors of iron oxides. Compared with Case 3, the reduction degrees of Case 1 and Case 2 in the shaft are generally higher at the same horizontal level. Additionally, for the case with a lighter burden batch weight, the CZ starts to form at a higher height. Thus, it is indicated that with a lighter burden, iron oxides can be reduced much faster; therefore, the reduction load, especially near the central furnace regions, decreases.

To be more quantitative, the reduction degree evolutions above CZs and along different vertical lines, *viz.* $x = 0$, $x = 2$ and $x = 5$, are shown in Figures 16(a) to (c), respectively. Note that the reduction degrees gradually increase; however, inside the coke layers they are zero where no iron oxides exist. These figures clearly show that, at the same heights, the reduction degrees of iron oxides with a more massive burden batch weight are smaller than those with a small one. Comparing Figures 16(a) through (c) shows that with the decreasing of ore particles, the reduction degree difference increases, and the difference at the same height can be as large as 0.5 at some points. It proves that the reduction load inside the BF becomes heavier with the increased burden batch weight, particularly near the furnace center. In other words, to reach the same reduction degree, iron oxides should travel a longer

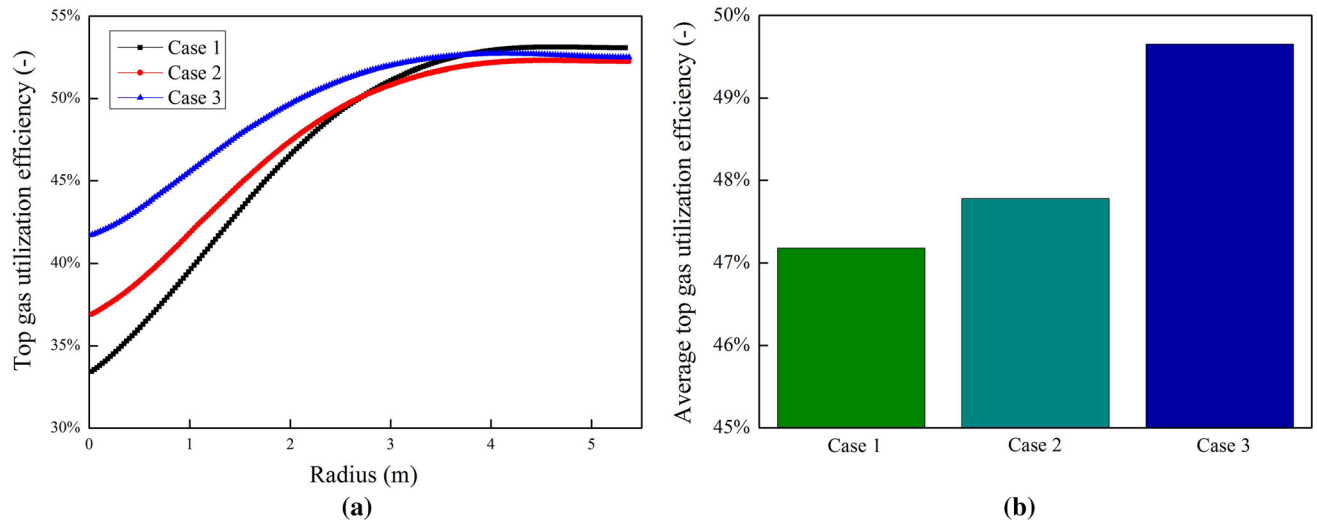


Fig. 14—Trends of top gas utilization efficiency along the furnace radial direction (a) and the distributions of average top gas utilization efficiency (b).

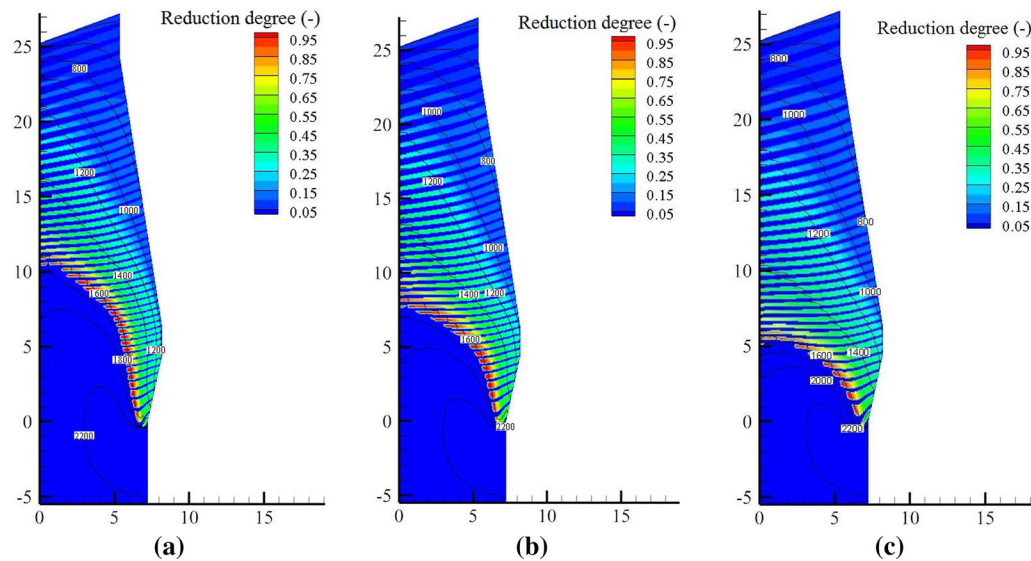


Fig. 15—Reduction degree distributions of the three cases with different burden batch weights: (a) Case 1: 112 tons; (b) Case 2: 126 tons and (c) Case 3: 140 tons.

distance inside the BF with a large burden batch weight. Thus, for extremely large burden batch weights, iron oxides might not be reduced well before entering, such as the dripping zone and stagnant region. To make a better comparison of the reduction development of the three cases, the average reduction degree along the radial direction is calculated and plotted in Figure 16(d), respectively. The calculation scheme is similar to Eq. [10], but with the reduction degree of iron oxides adopted instead of gas velocity. These reduction degree curves show similar distribution trends. Specifically, the average reduction degree decreases first with an increased radius and reaches the respective valley of ~ 0.22 at a radius of 5.5 m. The difference in the average reduction degree near the furnace center can be ~ 0.05 .

However, compared with the previous average gas velocity and phase temperature, the curves in Figure 16 show unobvious trends near the central furnace regions. It is because the average reduction degree is affected not only by the reduction degree in the ore layers, but also the iron ore cell numbers in the shaft. Specifically, the CZ location (Figures 8 and 15) is different near the furnace center, making the local trends become ambiguous. On the other hand, the trends of reduction degree become much clearer near the furnace wall where the CZ profiles show relatively unobvious changes. Near the peripheral regions, the average reduction degree of Case 3 is the lowest, indicating the reduction load of a BF in the peripheral regions increases with a larger batch weight.

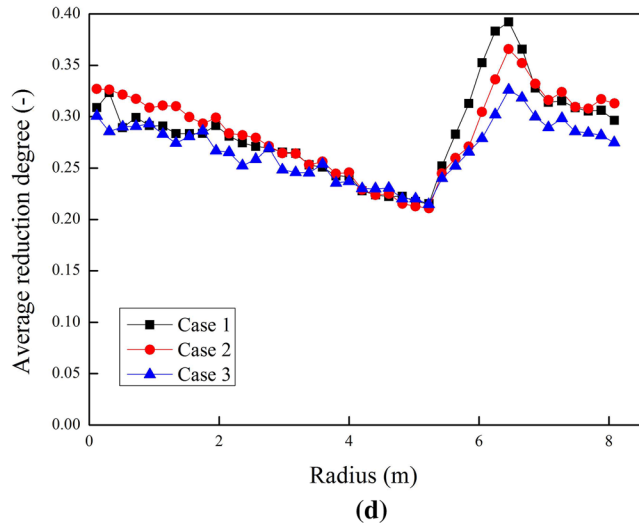
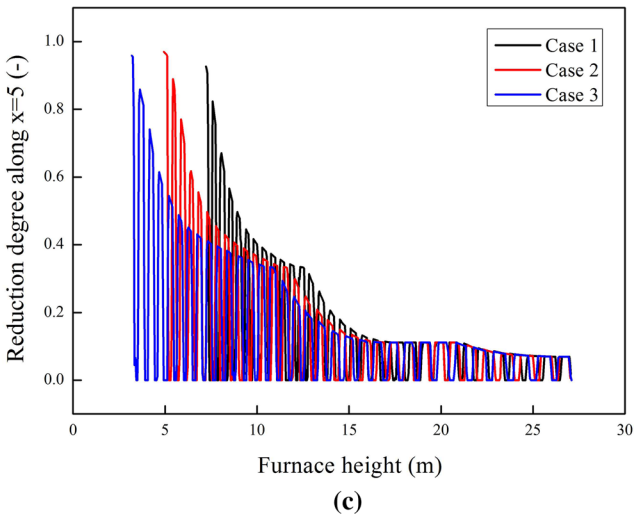
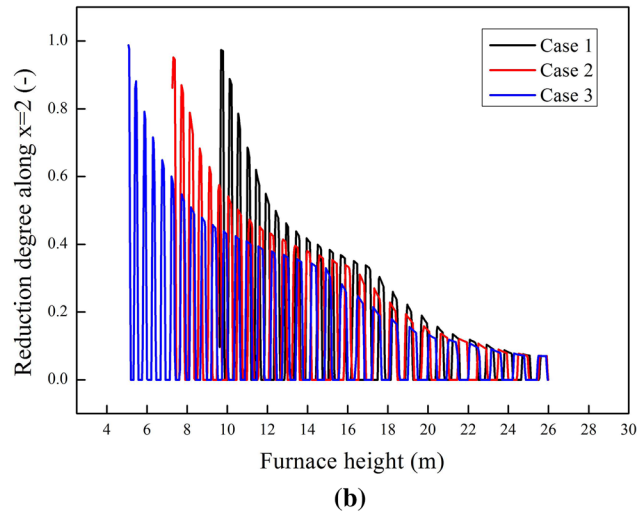
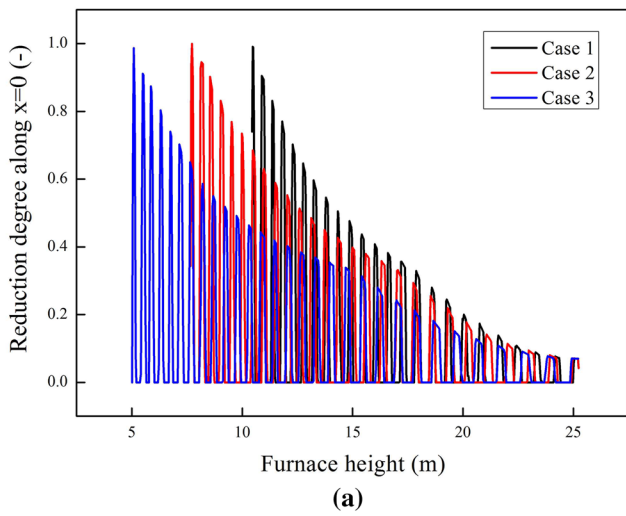


Fig. 16—Reduction degree evolution: (a) to (c) along the lines of $x = 0$, $x = 2$ and $x = 5$ and (d) the average reduction degrees along the furnace radial direction.

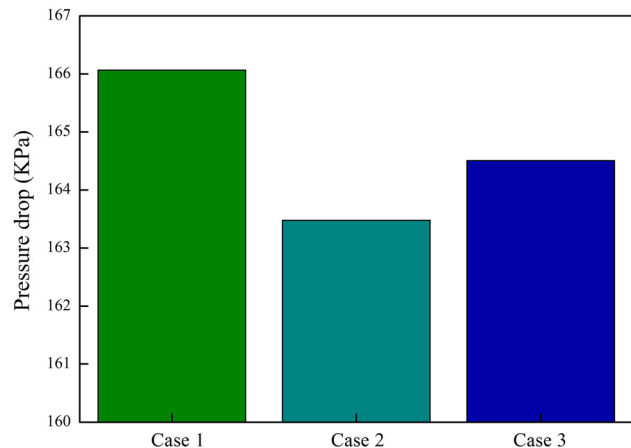
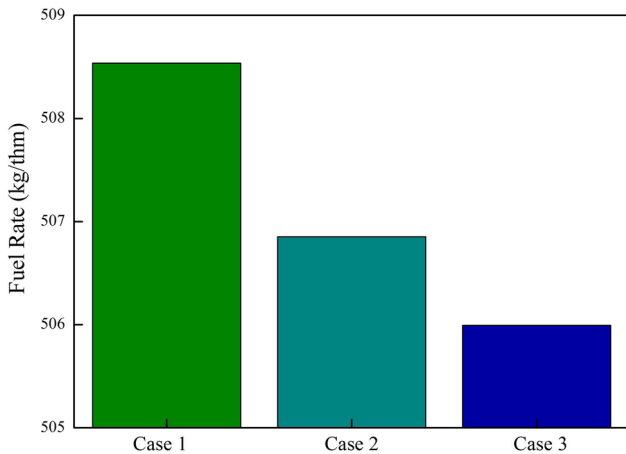


Fig. 17—Fuel rates of the three cases with different burden batch weights: (Case 1), 112 tons; (Case 2), 126 tons and (Case 3), 140 tons.

Fig. 18—Pressure drops of the three cases with different burden batch weights: (Case 1), 112 tons; (Case 2), 126 tons and (Case 3), 140 tons.

B. Key Performance Indicators

1. Fuel rate

Figure 17 compares the fuel rates of the three cases. It is noted that with the increased ore batch weight, the fuel rate shows a clear decreasing trend, from ~ 508.5 to ~ 506.0 kg/thm. A decrease of ~ 2.5 kg/thm is observed. From the viewpoint of fuel rate saving, the BF operation with a large ore batch weight should be recommended. However, as discussed in the previous sections, the declined position of the CZ, together with the decreased central gas velocity, can co-exist when a BF adopts a large batch weight. Thus, the raw materials far away from gas inlets might not be reduced well, and the accumulation of raw materials could take place under some extremely heavy burdens. Thus, a chill hearth could be formed finally. Therefore, the increased batch weight should be carefully selected to balance the increased gas blow ability and increased raw material quality.

2. Gas permeability

The blast furnace permeability index is an empirical parameter with various expressions but basically relates to the furnace pressure drop and bosh gas flow rate. In this study, the bosh gas flow rate is constant. Therefore, furnace permeability can be directly reflected by analyzing the furnace pressure drop. The result (Figure 18) indicates that with the increased burden batch weight from Cases 1 to 3, Case 2 shows a lower pressure drop, indicating the fluctuations of furnace permeability. The reason behind these phenomena should be the change of gas flow patterns in different regions brought by the different porosities and gas permeabilities. It is concluded that the relationship between BF permeability and burden batch weight is not a simple linear and might need further study, *e.g.*, using as CFD-DEM approach.

V. CONCLUSIONS

A mathematical BF model based on multi-fluid theory is adopted to investigate the influence of burden batch weight on BF in terms of inner phenomena and performance, including gas flow patterns and thermal-chemical behaviors, CZ shape and location, reducing gas evolution and iron oxide reduction distribution, fuel rate and gas permeability. The key findings of this study are as follows:

1. Burden batch weight has a significant effect on the gas flow field. When the batch weight increases from 112 to 140 tons, the average gas velocity near the furnace center decreases by 1 m/s while that near-periphery bosh regions increase.
2. The thermal condition is significantly affected by the burden batch weight. With the increased batch weight, both the average temperature of the gas phase and solid phase declines by roughly 160 K; the CZ position descends by ~ 7 m near the BF center. Besides, the reduction load is expected to become

heavier inside the BF, particularly by ~ 0.05 near the BF center.

3. Both the top gas utilization and fuel rate can be affected by the batch weight. With the increased batch weight, the usage of reducing gas improves by ~ 2.5 pct with the decreased fuel rate by ~ 2.5 kg/thm, *viz.*, the furnace efficiency can be improved with a more considerable burden batch weight.

In summary, a large batch weight is recommended in view of furnace efficiency. Meanwhile, the development of central gas flow should be ensured for stability.

This work quantitatively investigates the influence of batch weight on the BF performance, which is expected to provide theoretical support for the batch weight selection in practice.

ACKNOWLEDGMENTS

The authors acknowledge the financial support from the Australian Research Council (LP160101100), Coal Energy Australia, and Baosteel. The first author extends his gratitude to the China Scholarship Council for financial support.

REFERENCES

1. X. Wang, S. Wang, and J. Chen: *Ironmaking*, 2009, vol. 28, pp. 8–11.
2. Y. Omori: *Blast Furnace Phenomena and Modelling*, Elsevier Applied Science, London, 1987, p. 498.
3. K. Kanbara, T. Hagiwara, A. Shigemi, S. Kondo, Y. Kanayama, K. Wakabayashi, and N. Hiramoto: *Tetsu-to-Hagané*, 1976, vol. 62, pp. 535–46.
4. K. Kojima, T. Nist, T. Yamaguchi, H. Nakama, and S. Ida: *Tetsu-to-Hagané*, 1976, vol. 62, pp. 570–79.
5. K. Sasaki, M. Hatano, M. Watanabe, T. Shimoda, K. Yokotani, T. Ito, and T. Yakoi: *Tetsu-to-Hagané*, 1976, vol. 62, pp. 580–91.
6. M. Sasaki, K. Ono, A. Suzuki, Y. Okuno, K. Yoshizawa, and T. Nakamura: *Tetsu-to-Hagané*, 1976, vol. 62, pp. 559–69.
7. Y. Shimomura, K. Nishikawa, S. Arino, T. Katayama, Y. Hida, and T. Isoyama: *Tetsu-to-Hagané*, 1976, vol. 62, pp. 547–58.
8. K. Narita, T. Sato, M. Maekawa, S. Fukihara, H. Kanayama, and S. Sasahara: *Tetsu-to-Hagané*, 1980, vol. 66, pp. 1975–84.
9. M. Geerdes, R. Chaigneau, and I. Kurunov: *Modern Blast Furnace Ironmaking: An Introduction*, IOS Press, Amsterdam, 2015, p. 16.
10. L. Yuncai: *Blast furnace burden distribution*, Metallurgical Industry Press, Beijing, 2005, p. 62.
11. H. Mio, M. Kadowaki, S. Matsuzaki, and K. Kunitomo: *Miner. Eng.*, 2012, vol. 33, pp. 27–33.
12. D. Fu, Y. Chen, and C.Q. Zhou: *Appl. Math. Model.*, 2015, vol. 39, pp. 7554–67.
13. J. Jimenez, J. Mochón, A. Formoso, and J.S. de Ayala: *ISIJ Int.*, 2000, vol. 40, pp. 114–20.
14. C.K. Ho, S.M. Wu, H.P. Zhu, A.B. Yu, and S.T. Tsai: *Miner. Eng.*, 2009, vol. 22, pp. 986–94.
15. Y.S. Shen, A.B. Yu, and P. Zulli: *Steel Res. Int.*, 2011, vol. 82, pp. 532–42.
16. F.M. Shen, B. Sundelin, K. Paulsson, E. Kapilashrami, G. Wei, M.S. Chu, and Y.S. Shen: *Steel Res. Int.*, 2008, vol. 79, pp. 11–6.
17. Z. Miao, Z. Zhou, A.B. Yu, and Y. Shen: *Powder Technol.*, 2017, vol. 314, pp. 542–49.
18. X. Hao, F. Shen, G. Du, Y. Shen, and Z. Xie: *Steel Res. Int.*, 2005, vol. 76, pp. 694–99.
19. J. Hinnelä and H. Saxén: *Comput.*, 2003, vol. 14, pp. 677–82.

20. J.I. Park, U.H. Baek, K.S. Jang, H.S. Oh, and J.W. Han: *ISIJ Int.*, 2011, vol. 51, pp. 1617–23.
21. J.I. Park, H.J. Jung, M.K. Jo, H.S. Oh, and J.W. Han: *Met. Mater. Int.*, 2011, vol. 17, pp. 485–96.
22. Q. Zhu, C.L. Lv, Y.X. Yin, and X.Z. Chen: *J. Iron Steel Res. Int.*, 2013, vol. 20, pp. 33–37.
23. H.F. Li, H. Saxén, W.Q. Liu, Z.S. Zou, and L. Shao: *Metals*, 2019, vol. 9, pp. 1–18.
24. V.R. Radhakrishnan and K.M. Ram: *J. Process Contr.*, 2001, vol. 11, pp. 565–86.
25. H. Nishio and T. Ariyama: *Tetsu-to-Hagané*, 1982, vol. 68, pp. 2330–37.
26. M. Nikus and H. Saxén: *ISIJ Int.*, 1996, vol. 36, pp. 1142–50.
27. F. Pettersson, J. Hinnela, and H. Saxén: *Mater. Manuf. Process.*, 2003, vol. 18, pp. 385–99.
28. Y. Yang, Y. Yin, D. Wunsch, S. Zhang, X. Chen, X. Li, S. Cheng, M. Wu, and K.Z. Liu: *ISIJ Int.*, 2017, vol. 57, pp. 1350–63.
29. X. Yu and Y. Shen: *Metall. Mater. Trans. B*, 2019, vol. 50B, pp. 2238–50.
30. X. Yu and Y. Shen: *Powder Technol.*, 2020, vol. 361, pp. 124–35.
31. X. Yu and Y. Shen: *Energy Fuels*, 2019, vol. 33, pp. 11603–616.
32. T. Mitra and H. Saxén: *Metall. Mater. Trans. B*, 2014, vol. 45B, pp. 2382–94.
33. S. Wu, M. Kou, J. Xu, X. Guo, K. Du, W. Shen, and J. Sun: *Chem. Eng. Sci.*, 2013, vol. 99, pp. 314–23.
34. Y. Yu and H. Saxén: *Chem. Eng. Sci.*, 2010, vol. 65, pp. 5237–50.
35. T. Mitra and H. Saxén: *IFAC-PapersOnLine*, 2015, vol. 48, pp. 183–88.
36. J.L. Zhang, Y.X. Chen, Z.Y. Fan, Z.W. Hu, T.J. Yang, and T. Ariyama: *J. Iron Steel Res. Int.*, 2011, vol. 18, pp. 1–6.
37. W.J. Yang, Z.Y. Zhou, and A.B. Yu: *Chem. Eng. J.*, 2015, vol. 278, pp. 339–52.
38. Z. Zhou, H. Zhu, A. Yu, and P. Zulli: *ISIJ Int.*, 2010, vol. 50, pp. 515–23.
39. S.B. Kuang, Z.Y. Li, and A.B. Yu: *Steel Res. Int.*, 2018, vol. 89, pp. 1–25.
40. F. Bambauer, S. Wirtz, V. Scherer, and H. Bartusch: *Powder Technol.*, 2018, vol. 334, pp. 53–64.
41. Q. Hou, S. Kuang, Z. Li, and A.B. Yu: *Powder Technol.*, 2017, vol. 314, pp. 557–66.
42. X. Yu and Y. Shen: *Metall. Mater. Trans. B*, 2018, vol. 49B, pp. 2370–88.
43. X. Yu and Y. Shen: *Chem. Eng. Sci.*, 2019, vol. 199, pp. 50–63.
44. P.R. Austin, H. Nogami, and J. Yagi: *ISIJ Int.*, 1997, vol. 37, pp. 458–67.
45. G.X. Wang, S.J. Chew, A.B. Yu, and P. Zulli: *Metall. Mater. Trans. B*, 1997, vol. 28B, pp. 333–43.
46. W.E. Ranz and W.R. Marshall: *Chem. Eng. Prog.*, 1952, vol. 48, pp. 141–46.
47. E.R.G. Eckert and R.M. Drake: *Heat and Mass Transfer*, 2nd ed., McGrawHill, New York, 1959.
48. P.J. Mackey and N.A. Warner: *Metall. Trans.*, 1972, vol. 3, pp. 1807–16.
49. D. Maldonado, Ph. D. UNSW, 2003.
50. I. Muchi: *Trans. ISIJ.*, 1976, vol. 7, pp. 223–37.
51. P.R. Austin, H. Nogami, and J. Yagi: *ISIJ Int.*, 1997, vol. 37, pp. 748–55.
52. J.A.D. Castro, H. Nogami, and J. Yagi: *ISIJ Int.*, 2002, vol. 42, pp. 44–52.
53. H. Nogami, M.S. Chu, and J. Yagi: *Comput. Chem. Eng.*, 2005, vol. 29, pp. 2438–48.
54. X.F. Dong, A.B. Yu, S.J. Chew, and P. Zulli: *Metall. Mater. Trans. B*, 2010, vol. 41B, pp. 330–49.
55. Y. Shen, B. Guo, S. Chew, P. Austin, and A.B. Yu: *Metall. Mater. Trans. B*, 2016, vol. 47B, pp. 1052–62.
56. Y. Shen, B. Guo, S. Chew, P. Austin, and A.B. Yu: *Metall. Mater. Trans. B*, 2014, vol. 46B, pp. 432–48.
57. O. Yucel, F. Demirci, A. Turan, and M. Alkan: *High Temp. Mat.*, 2013, vol. 32, pp. 405–12.

Publisher's Note Springer Nature remains neutral with regard to jurisdictional claims in published maps and institutional affiliations.